



## Finite-element simulations of the pH-ElecFET microsensors

Nejiba Aoun, Fraj Echouchene, Abdou Karim Diallo, Jérôme Launay, Pierre Temple-Boyer, Hafedh Belmabrouk

### ► To cite this version:

Nejiba Aoun, Fraj Echouchene, Abdou Karim Diallo, Jérôme Launay, Pierre Temple-Boyer, et al.. Finite-element simulations of the pH-ElecFET microsensors. IEEE Sensors Journal, 2016, 16 (17), pp.6519-6526. 10.1109/JSEN.2016.2585506 . hal-01503193

**HAL Id: hal-01503193**

**<https://hal.science/hal-01503193>**

Submitted on 6 Apr 2017

**HAL** is a multi-disciplinary open access archive for the deposit and dissemination of scientific research documents, whether they are published or not. The documents may come from teaching and research institutions in France or abroad, or from public or private research centers.

L'archive ouverte pluridisciplinaire **HAL**, est destinée au dépôt et à la diffusion de documents scientifiques de niveau recherche, publiés ou non, émanant des établissements d'enseignement et de recherche français ou étrangers, des laboratoires publics ou privés.

# Finite-element simulations of the pH-ElecFET microsenors

*N. Aoun, F. Echouchene, A. K. Diallo, J. Launay, P. Temple-Boyer and H. Belmabrouk*

**Abstract**—This paper presents a COMSOL Multiphysics 2D axisymmetric model of an pH-ElecFET (pH-sensitive electrochemical field effect transistor) microsensor. This device combines an integrated microelectrode with a pH-sensitive chemical field effect transistor (pH-ChemFET). Thus, by triggering electrolysis phenomena owing to the integrated microelectrode, associated local pH variations in microvolumes are monitored thanks to the pH-ChemFET microdevice. Taking into account (electro) chemical reactions and diffusion phenomena in liquid phase, the proposed model points out the role of the ElecFET geometrical design (microelectrode width  $w$ , gate sensitive radius  $r_e$  and distance between the pH-ChemFET gate and the microelectrode  $d$ ), as well as polarization parameters, (polarization voltage  $V_p$  and time  $t_p$ ), on the microsensor response. It is first applied to water electrolysis in order to validate pH impulsional variations in microvolume. Then, oxidation of hydrogen peroxide in phosphate buffer (PBS,  $\text{pH}_0=7.2$ ) solutions is studied, evidencing the  $\text{H}_2\text{O}_2$  potentiometric detection in the [10–100mM] concentration range. This developed model paves new ways for sensor applications, opening several new opportunities for pH-ElecFET devices for  $\text{H}_2\text{O}_2$ -related enzymatic detection of biomolecules.

**Index Terms**—Modelling, ElecFET, microelectrode, pH-ChemFET, water electrolysis, hydrogen peroxide detection.

## I. INTRODUCTION

In the last decade, the electrochemical microsensors have received an increasing interest in a wide range of applications such as clinical diagnostics, food analysis, environmental monitoring due to their low cost, simple operation, small size, and rapidity, sensitivity and real-time [1–3]. The electrochemical sensors can be divided into three groups depending on the measured electrical signal [4–6]: amperometric, potentiometric, and conductometric. Even so, the combination of amperometric and potentiometric techniques is a very promising method in terms of detection [7–10]. Diallo et al. have developed an electrochemical field effect transistor (ElecFET) microsensor based on this technique [8, 9]. This device is achieved through the integration of a planar noble metal electrode around the dielectric gate area of a pH-sensitive ChemFET microdevice. By triggering pH-related electrochemical reactions thanks to the microelectrode polarization and by monitoring the so-

obtained pH variations thanks to the pH-ChemFET, electrolysis phenomena and pH measurement are closely embedded at the microscale, enabling new electrochemical detection potentialities. Among the ElecFET microdevice applications, the most frequent is the manufacturing of a pH-related enzyme sensor. In this case, the ChemFET detects the pH change resulting from the enzymatic reaction in the membrane that covers the sensor [11]. The output voltage of the ChemFET controls the current flowing through the sensor-actuator system [12]. ElecFET has been successfully used to determine acid or base concentration [13], to form the heart of a carbon dioxide sensor [14] and detect different biomolecules [8, 11].

Various mathematical models of microsensors have been developed and successfully used to study and optimize analytical characteristics of microsensors [15–18]. Meena and Rajendran [15] have derived analytical expressions of concentration and current in order to describe and evaluate the performances of amperometric and potentiometric biosensors using homotopy perturbation method. A numerical study of potentiometric and amperometric electrochemical gas sensors based in a solid-state ion conducting electrolyte has presented by López-Gándaraa et al. [16] in order to optimize the diffuse layers covering one of their catalytic electrodes. The model describes the current-voltage characteristics in the system layer/electrode/electrolyte/electrode. A theoretical study and numerical simulation of potentiometric and amperometric enzyme electrodes and of enzyme reactors have been developed by Morf et al. [17, 18]. The response characteristics of potentiometric and amperometric sensor systems, as well as the product release from enzyme reactors, are analyzed, and the influence of the relevant parameters on the steady-state response is demonstrated and discussed [17].

In this paper, we apply the concept of the combination of amperometric and potentiometric techniques to simulate the ElecFET microdevice detection principles, in order to monitor water ( $\text{H}_2\text{O}$ ) electrolysis phenomena in a first stage and hydrogen peroxide ( $\text{H}_2\text{O}_2$ ) electrochemical detection in the second stage. We then focus on the study of the influences of the main parameters, i.e. (i) polarization voltage  $V_p$  and time  $t_p$  on the integrated microelectrode, (ii) characteristic of the microelectrode width  $w$ , (iii) distance between the gate sensitive radius and the integrated microelectrode  $d$  and (iv) gate sensitive radius  $r_e$ .

## II. PRESENTATION OF THE SIMULATION MODEL

The modelling approach used takes into account the different chemical, electrochemical and physical phenomena occurring in the frame of the ElecFET detection principles:

- Oxido-reduction on the integrated microelectrode;

N. Aoun and F. Echouchene are with the Laboratory of Electronics and Microelectronics, University of Monastir, 5000, Tunisia (e-mail: nejibaaoun@yahoo.com, frchouchene@yahoo.fr)

A. K. Diallo, J. Launay and Temple-Boyer are with the University of Toulouse, UPS, LAAS, F-31400 Toulouse, France.

H. Belmabrouk is with the Department of Physics, College of Science AlZulfi, Majmaah University, Saudi Arabia.

- Diffusion phenomena;
- ( $\text{H}_3\text{O}^+/\text{H}_2\text{O}$ ) and ( $\text{H}_2\text{O}/\text{OH}^-$ ) and acid-base analysis of aqueous solutions at  $\text{pH}_0=7.2$ .

The ElecFET detection properties were thus modeled by studying the diffusion phenomena of the main chemical species in the electrolyte, focusing on the  $\text{H}_3\text{O}^+/\text{OH}^-$  water-based ions, and finally by analyzing the pH detection properties of the silicon nitride  $\text{Si}_3\text{N}_4$  ChemFET gate.

#### A. Geometry of ElecFET: comparison between real and simulated model

Since their fabrication process used silicon-based microtechnologies and therefore photolithography, the real ElecFET microdevices are based on a rectangular concentric geometry [9]. In order to decrease calculation times, the simulated model was simplified by using  $r$ - $z$  cylindrical geometry, leading to a 2D axisymmetric geometry (Fig. 1).

The geometrical parameters are: the gate sensitive radius  $r_e$ , the distance between the sensitive gate and the electrode  $d$ , and  $w$  the microelectrode ring width. The depth of the sensitive gate  $z_e$  is  $0.5\mu\text{m}$  and the height of the modeled geometry is  $h=300\mu\text{m}$ . The standard values of the parameters ( $r_e$ ,  $d$ ,  $w$ ) are ( $10\mu\text{m}$ ,  $50\mu\text{m}$ ,  $100\mu\text{m}$ ). At the end of the paper these values will be modified in order to enhance the performance of pH-ElecFET. The dimensions of electrolyte domain are indicated in Fig. 1.

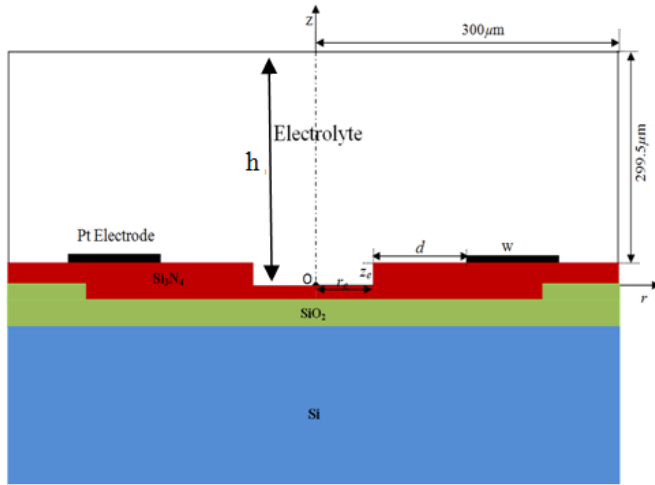
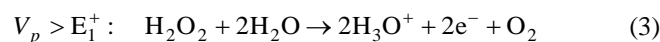
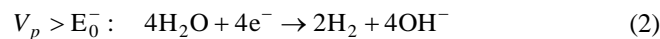
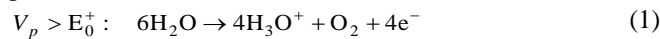


Fig. 1. Cross-section of the ElecFET device in  $r$ - $z$  cylindrical coordinates.

#### B. Modelling of the electrochemical reactions ( $\text{H}_2\text{O}$ & $\text{H}_2\text{O}_2$ )

The ElecFET concept was initially used for the monitoring of water ( $\text{H}_2\text{O}$ ) hydrolysis and secondly of the hydrogen peroxide ( $\text{H}_2\text{O}_2$ ) oxidation in water based solutions:



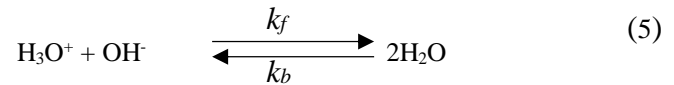
where  $E_0^+$ ,  $E_0^-$ , and  $E_1^+$  are equilibrium potentials of the  $\text{O}_2/\text{H}_2\text{O}$ , the  $\text{H}_2/\text{H}_2\text{O}$  and  $\text{O}_2/\text{H}_2\text{O}_2$  redox couple, respectively. The values of the constants are:  $E_0^+ = 1.2\text{V}$ ,  $E_0^- = -0.8\text{V}$  [9] and  $E_1^+ = 0.7\text{V}$  [8].

#### C. Modelling of the diffusion phenomena in water

Diffusion phenomena of the most influential chemical species, i.e.  $\text{H}_3\text{O}^+$  and  $\text{OH}^-$  ions in case of  $\text{H}_2\text{O}$  detection and  $\text{H}_3\text{O}^+$ ,  $\text{OH}^-$  and  $\text{H}_2\text{O}_2$  species in case of hydrogen peroxide detection, into water, have been modeled using the Fick law:

$$\frac{\partial c_i}{\partial t} = D_i \left( \frac{\partial^2 c_i}{\partial r^2} + \frac{1}{r} \frac{\partial c_i}{\partial r} + \frac{\partial^2 c_i}{\partial z^2} \right) + R_i \quad (4)$$

where  $t$  denotes the time,  $c_i$  is the concentration of the studied chemical species,  $D_i$  is its diffusion coefficient and  $R_i$  is an additional term accounting for the production/consumption rate of the ion species through a possible chemical reaction. The reaction term can be deduced using the water protolysis reaction:



where  $k_f$  and  $k_b$  are the forward and backward reaction kinetic rates, respectively.

One can thus express the reaction for the production of proton and hydroxide ions as [19]:

$$\begin{aligned} R_{\text{H}_3\text{O}^+} &= R_{\text{OH}^-} = k_b[\text{H}_2\text{O}] - k_f[\text{H}_3\text{O}^+][\text{OH}^-] \\ &= k_f \left( K_e - [\text{H}_3\text{O}^+][\text{OH}^-] \right) \end{aligned} \quad (6)$$

where  $K_e = k_b[\text{H}_2\text{O}]/k_f$  is the equilibrium constant of water.

The forward rate constant  $k_f$  of the water protolysis reaction is estimated by values taken from literature [20] while the backward rate constants  $k_b$  is obtained from where  $K_e$  denotes the water dissociation constant.

Buffer solution is of great importance in biosensor applications. Experimentally, the buffer concentration could be optimized. So, a lot of experiments have been reported on the buffer properties which enhance the response and the stability of the biosensor [21, 22]. In our kinetic model the chemical effect of the buffer solution was neglected and was not taken into account. In the frame of a kinetic approach, the influences of acid/bases other than the water-based ones are limited by diffusion phenomena (Eq. 4). In another way, we have been interested only on the protonation reaction because, as a solvent, water is in excess in solution. As a result, we can assume that the buffer solution does not have an effect on the biosensor response which can be expressed with the chemical effect modeled with physical equations.

#### D. Initial and boundary conditions

Boundary conditions are crucial for a correct description of phenomena with partial differential equations. For our model, several important conditions have to be set. The initial condition related to mass transport of species is given by:

$$\begin{cases} c_{\text{H}_3\text{O}^+}(r, z; t=0) = 10^{-\text{pH}_0} \\ c_{\text{OH}^-}(r, z; t=0) = 10^{-\text{pK}_e + \text{pH}_0} \\ c_{\text{H}_2\text{O}_2}(r, z; t=0) = 50\text{mM} \end{cases} \quad \begin{cases} 0 \leq r \leq 300\mu\text{m} \\ 0 \leq z \leq h \end{cases} \quad (7)$$

On the axis of symmetry, the boundary condition reads:

$$\frac{\partial c_i}{\partial r}(r=0, z, t) = 0 \quad (8)$$

At the upper interface of the electrolyte ( $z=h$ ) and the lower interface ( $z=0$  or  $z_e$ ), the interface is assumed to be impermeable:

$$\frac{\partial c_i}{\partial z}(r, z=h \text{ or } 0 \text{ or } z_e, t) = 0 \quad (9)$$

In order to do not disturb the diffusion phenomena operating from the surface of the microelectrode, the outer surface of the device is assumed to be at a constant concentration:

$$c_i(r = 300 \mu\text{m}, z, t) = c_{i,0} \quad (10)$$

An oxido-reduction reaction takes place at the electrode for  $t < t_p$ . Thus, the boundary condition reads:

$$D_i \frac{\partial c_i}{\partial z}(r, z=z_e, t \leq t_p) = \frac{\nu_{i,j}}{N_j F} i_j ; \quad r_e + d \leq r \leq r_e + d + w \quad (11)$$

where  $N_j$  is the number of electron transferred for reaction “j”,  $\nu_{i,j}$  is the stoichiometric coefficient,  $F$  is Faraday’s constant and  $t_p$  is the polarization time.  $i_j$  denotes the current density given from the kinetic equations for the electrochemical reactions at the electrode surface based on the Butler–Volmer expression[23]:

$$i_j = i_{0j,ref} \left\{ \prod_i \left( \frac{c_i}{c_{i,ref}} \right)^{p_{i,j}} \exp\left(\frac{\alpha_{a,j} F}{RT} \eta_j\right) - \prod_i \left( \frac{c_i}{c_{i,ref}} \right)^{q_{i,j}} \exp\left(-\frac{\alpha_{c,j} F}{RT} \eta_j\right) \right\} \quad (12)$$

where  $i_{0j,ref}$  is the exchange current density due to reaction “j” at the reference concentrations in  $\text{A}/\text{cm}^2$ ,  $c_i$  is the concentration of species “i” adjacent to the surface of electrode in  $\text{mol}/\text{cm}^3$ ,  $c_{i,ref}$  is the reference concentration of species “i” in  $\text{mol}/\text{cm}^3$ ,  $\alpha_{aj}$  is the anodic transfer coefficient for reaction “j”,  $\alpha_{cj}$  is the cathodic transfer coefficient for reaction “j”,  $p_{i,j} = \nu_{i,j}$  is the anodic reaction order of species “i” in reaction “j”,  $q_{i,j} = -\nu_{i,j}$  is the cathodic reaction order of species “i” in reaction “j”,  $R$  is the gas constant,  $T$  is the temperature and  $\eta_j$  is the overpotential of reaction “j” in volts (V), and it is measured with respect to a reference electrode of a given kind in a solution at the reference concentrations.

The overpotential for electrochemical reaction “j”, ( $\eta$ ) in Eq. 12 is given by:

$$\eta_j = V_p - E_{0,j} \quad (13)$$

where  $V_p$  is the applied potential surface in V,  $E_{0,j}$  is the equilibrium potential for reaction “j”.

Total current is obtained by numerical integration of the local current density over the entire ElecFET area. It is given by:

$$I(t) = \int_A i_j dA \quad (14)$$

where  $A$  is the surface area of the electrode.

### E. Numerical method

The governing equations with initial and boundary conditions are solved numerically using the finite element software COMSOL Multiphysics 4.3b [24]. An electroanalysis module has been chosen for solving the mass transport of diluted species in electrolytes using the diffusion equation.

The overall computational domain is discretized using an unstructured triangular mesh Fig.2. It is noticed that the region nearby the reaction surface is refined with a better mesh quality.

For the time discretization we have employed First-order backward differentiation formula (BDF), with the time steps controlled by the numerical solver during the computations.

Total current, given by Eq. (14), is performed using a fourth order integration method.

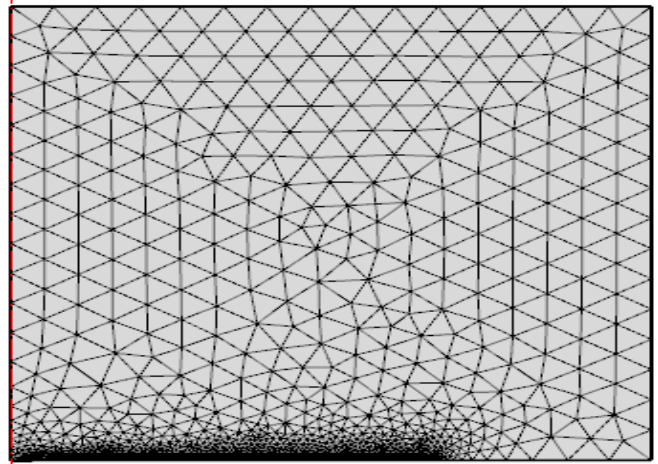


Fig. 2. Two-dimensional unstructured mesh with triangular elements.

## III. RESULTS AND DISCUSSION

To describe the *pH-ChemFET response*, we can use the threshold voltage variation. The pH-ElecFET threshold voltage variation is related to the pH at the silicon nitride  $\text{Si}_3\text{N}_4$  surface according to the following equation [20]:

$$V_T(t) = V_{T0} + s_0 \times (\text{pH}(0,t) - \text{pH}_{\text{pzc}}) \quad (15)$$

where  $\text{pH}(0,t)$  is the pH at the  $\text{Si}_3\text{N}_4$  sensitive surface when the diffusion phenomena “steady state” is reached and  $V_{T0}$  is a constant parameter depending on the  $\text{SiO}_2/\text{Si}_3\text{N}_4$  pH-ChemFET technology [25],  $\text{pH}_{\text{pzc}}$  is the point zero of charge which is estimated around 4 for  $\text{Si}_3\text{N}_4$  [23, 26]). In the following, since the  $V_{T0}$  value is only related to the pH-ChemFET technological fabrication, it is of no influence concerning the ElecFET detection properties and it will not be taken into account, i.e. it will be chosen equal to zero [27, 28].  $s_0$  is an ideal sensitivity of ISFET based pH sensor when pH is measured by the means of Nernst potential given by the following equation [29]:

$$s_0 = \frac{kT}{q} \ln(10) = 59.2 \text{ mV} / \text{pH} \quad (16)$$

where  $k=1.38 \times 10^{-23} \text{ J/K}$  is the Boltzmann constant,  $T=300 \text{ K}$  is temperature and  $q=1.6 \times 10^{-19} \text{ C}$  the elementary charge.

#### A. Mesh sensitivity

To ensure that the convergence has been obtained and the numerical results are independent of the mesh size, Fig. 3 shows the pH local at  $z=150 \mu\text{m}$  of the electrolyte for several mesh grids. There was no significant difference between the curves obtained using these grids (6818, 13643, 27719, 53534 elements) and we may conclude that the numerical convergence has been reached with all the grids. In the results section, all simulations were done with a total elements number 13645 [30, 31].

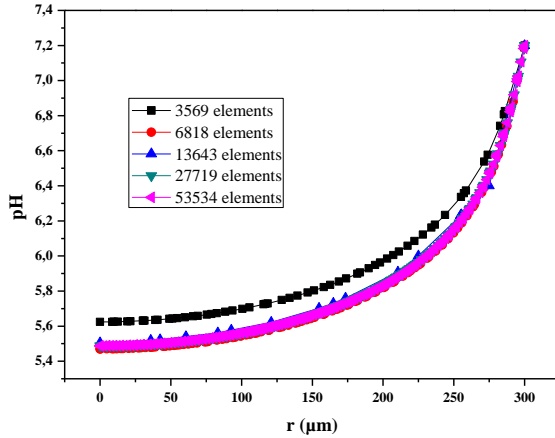


Fig. 3. pH at  $z = 150 \mu\text{m}$  of the electrolyte for several mesh grids.

#### B. Study of the most influential parameters

The kinetic parameters and the constants used in this simulation are listed in Table I and Table II [9, 32, 33]. ElecFET detection/transduction principles were first studied for water electrolysis monitoring  $\text{H}_2\text{O}$  in aqueous solutions ( $\text{pH}_0=7.2$ ). Then, the ElecFET detection properties were tested for the hydrogen peroxide  $\text{H}_2\text{O}_2$  also in aqueous solutions ( $\text{pH}_0=7.2$ ) solutions containing different stabilized concentrations  $[\text{H}_2\text{O}_2]$  ranging from 10 to 100mM because of their properties in terms of activity, stability and cost. According to theoretical equations, the most influential parameters are the polarization voltage  $V_p$ , the time of polarization  $t_p$ , the concentration  $[\text{H}_2\text{O}_2]$ , the distance between the gate sensitive radius and the microelectrode (parameter  $d$ ), the surface of the microelectrode (associated with the parameter  $w$ ) and gate sensitive radius (parameter  $r_e$ ).

All series of simulation have been devoted to modelling the sensor response, i.e. the dependence of the threshold voltage versus time. The curves of this threshold voltage, measured at  $\text{pH}_0=7.2$ , are shown in Figs.4-9.

TABLE I  
PARAMETERS USED IN THE SIMULATIONS

	Reaction 1	Reaction 2	Reaction 3
$i_{0j,ref} (\text{A/m}^2)$	$1.115 \times 10^{-6}$	$10^{-6}$	$9.64 \times 10^{-6}$
$E_{0j} (\text{V})$	1.2	-0.8	0.7
$\alpha_{a,j}$	0.5	0.5	0.5
$\alpha_{c,j}$	0.5	0.5	0.5
$V_{\text{H}_3\text{O}^+}$	+1		+1
$V_{\text{OH}^-}$		+1	
$V_{\text{H}_2\text{O}_2}$			-1
$N_j$	4	4	2

TABLE II  
PHYSICO-CHEMICAL INPUT VALUES USED IN THE SIMULATION MODEL

Parameter	Value	Unit
F	96352	C/mol
$D_{\text{H}_3\text{O}^+}$	$9.3 \times 10^{-9}$	$\text{m}^2/\text{s}$
$D_{\text{OH}^-}$	$5.3 \times 10^{-9}$	$\text{m}^2/\text{s}$
$D_{\text{H}_2\text{O}_2}$	$3.1 \times 10^{-10}$	$\text{m}^2/\text{s}$
$c_{\text{H}_3\text{O}^+,ref}$	$10^{-\text{pH}_0}$	mol/L
$c_{\text{OH}^-,ref}$	$10^{\text{pH}_0 - 14}$	mol/L
$c_{\text{H}_2\text{O}_2,ref}$	$50 \times 10^{-3}$	mol/L
$\text{pH}_0$	7.2	
$k_f$	$1.5 \times 10^{11}$	L/mol/s
$K_e$	$1 \times 10^{-14}$	$\text{mol}^2/\text{L}^2$

#### Case1: water electrolysis monitoring:

Before testing the sensor performance for the  $\text{H}_2\text{O}_2$  detection, one should ensure that the sensor is able to provide a response in the case of water electrolysis.

Fig. 4 presents the temporal evolution of the threshold voltage  $V_T$  in the case of  $\text{H}_2\text{O}$  redox phenomena for different polarization voltages while maintaining a constant the polarization time ( $t_p = 5 \text{ s}$ ). Since  $V_p$  is positive (respectively negative), oxidation (respectively reduction) of  $\text{H}_2\text{O}$  takes place near the platinum microelectrode.

Therefore, a production of hydronium  $\text{H}_3\text{O}^+$  (respectively hydroxide  $\text{OH}^-$ ) ions, so for a local pH changes sharply and finally the threshold voltage  $V_T$  increases (respectively decreases). In this case, phenomena occur at higher than 1.2V (positive polarization) and/or lower than -0.8V (negative polarization) polarization voltages  $V_p$  according to the associated equilibrium potential values  $E_0^+$  and  $E_1^+$ .

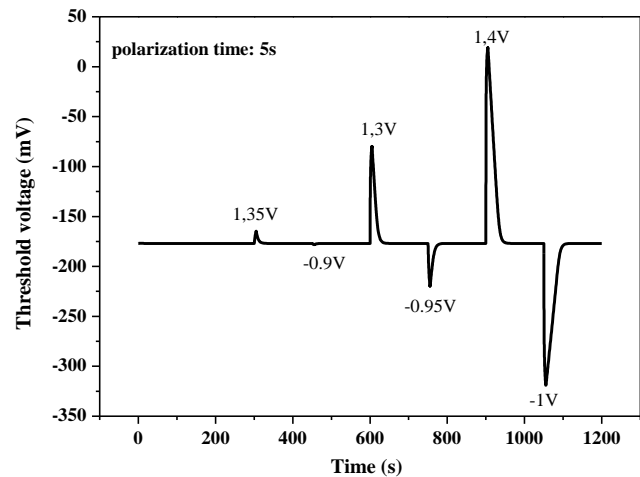


Fig. 4. Temporal variations of the pH-ChemFET threshold voltage for different polarization voltages.



The amplitude of the peak is so much greater than the value of the applied potential increases. When the polarization is interrupted, the ElecFET microsensor response follows a return to equilibrium of the system because of the diffusion laws.

Subsequently, the influence of polarization time  $t_p$  was studied. Fig. 5 illustrates the temporal variations threshold voltage for different polarization times ( $t_p = 5, 10, 10$  and  $3\text{ s}$ ) for two values of the polarization voltage on the integrated microelectrode ( $V_p = 1.4$  or  $-1\text{ V}$ ). In agreement with the Equation (11), the polarization time increase is responsible for a local pH decrease and therefore a pH-ChemFET threshold voltage increases (Eq. 15). Nevertheless, threshold voltage variations are lower and tend to reach saturation. Fig. 4 and Fig. 5 show clearly that the microsensor has a response in the case of water electrolysis. Therefore, we can continue our analysis and assess the performance of the sensor for  $\text{H}_2\text{O}_2$  detection.

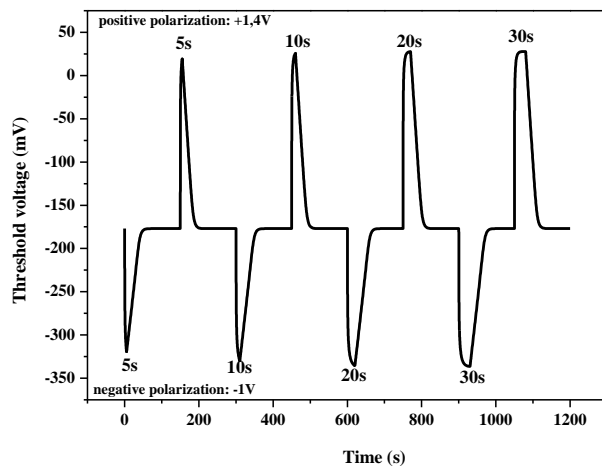


Fig. 5. Temporal variations of the pH-ChemFET threshold voltage for different polarization times.

#### Case2: hydrogen peroxide detection:

The ElecFET concept was studied by taking into account the  $\text{H}_2\text{O}_2$  oxidation on the integrated microelectrode. According to the oxidation reaction (Eq.3), in presence of hydrogen peroxide  $\text{H}_2\text{O}_2$ , a positive polarization  $V_p$  on the platinum microelectrode produces hydronium  $\text{H}_3\text{O}^+$  ions. Therefore, the local pH decreases around the sensitive area of the microsensor and finally the threshold voltage  $V_T$  increases. For this purpose, the polarization voltage  $V_p$  was chosen less than  $E_0^+$  to avoid any interference with water hydrolysis. Since the  $E_1^+$  is roughly equal to  $0.7\text{ V}$ , a similar polarization voltage  $V_p$  was applied on the platinum microelectrode at the different polarization times ( $t_p = 5, 10, 15, 20, 30, 40$  and  $60\text{ s}$ ) while keeping constant  $[\text{H}_2\text{O}_2]$  concentration at  $50\text{ mM}$  in a solution of  $\text{pH}_0=7.2$ , with a constant polarization voltage (Fig. 6).  $V_T$  tends toward increasingly positive values (i.e local pH decreases). As previously for the water electrolysis, the amplitude of the peaks increases with  $t_p$ . The maximum threshold voltage increases steeply over a short period of time and thereafter reaches a plateau value. It is clear that the

influence of polarization time appears only in transient state. The equilibrium state is reached for  $t_p=10\text{ s}$ .

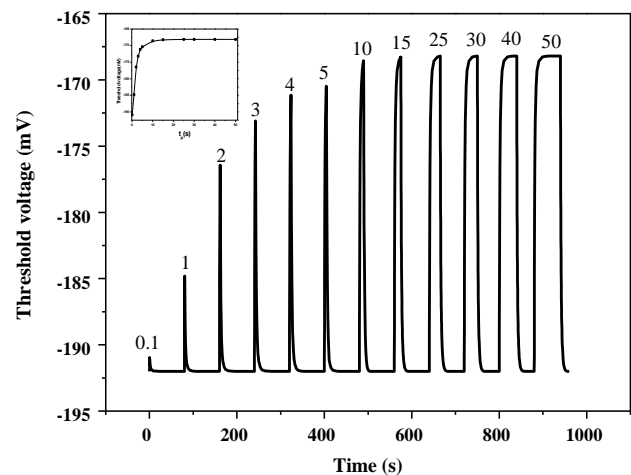


Fig. 6. Temporal variations of the pH-ChemFET threshold voltage for the different polarization times at  $[\text{H}_2\text{O}_2] = 50\text{ mM}$ ,  $V_p = 0.7\text{ V}$ ,  $d=50\mu\text{m}$ ,  $w=100\mu\text{m}$  and  $r_e=10\mu\text{m}$  and (inset) ElecFET response versus  $t_p$ .

In the same way, Fig. 7 represents the  $\text{H}_2\text{O}_2$ -ElecFET response as a function of time for different polarization voltages  $V_p$ . This figure has been obtained with  $[\text{H}_2\text{O}_2] = 50\text{ mM}$  in a solution of  $\text{pH}_0=7.2$  and  $t_p = 30\text{ s}$ .

We found that the asymptotic value of threshold voltage is essentially linearly related to the polarization voltage  $V_p$ . As soon as the polarization is interrupted, the ElecFET microsensor response tends to turn to back equilibrium of the system because of diffusion phenomenon. In the case of hydrogen peroxide detection, the Butler-Volmer theory emphasizes on the influence of the  $[\text{H}_2\text{O}_2]$  concentration of  $\text{H}_3\text{O}^+$  ion production kinetics (Eq. 3).

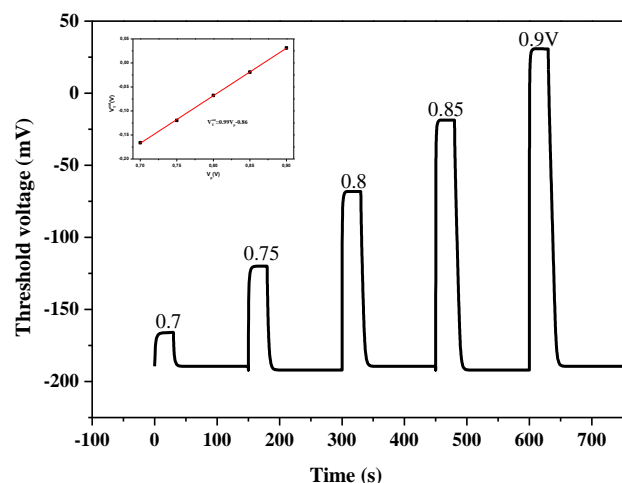


Fig. 7. Temporal variations of the pH-ChemFET threshold voltage for the different polarization voltages at  $[\text{H}_2\text{O}_2] = 50\text{ mM}$ ,  $t_p=30\text{ s}$ ,  $d=50\mu\text{m}$ ,  $w=100\mu\text{m}$  and  $r_e=10\mu\text{m}$  and (inset) ElecFET response  $V_p$ .

Fig. 8 shows temporal variations of the pH-ChemFET threshold voltage for different  $\text{H}_2\text{O}_2$  concentrations. Simulation results prove that the amplitude of the threshold voltage increases with the  $[\text{H}_2\text{O}_2]$  concentration in solution, and saturates for the highest values. This saturation

phenomenon is related to the previously discussed ElecFET detection principles [33].

Fig. 8 inset presents the evolution of the asymptotic threshold voltage  $V_T^{Sat}$  versus the concentration  $[H_2O_2]$  and at  $V_p=0.7V$  and  $t_p=30s$ . As illustrated in Fig. 8 inset, the simulation shows a linear response through a large range of  $[H_2O_2]$  concentration, as well as a very insensitive behavior. The influence of the microelectrode positions, the surface of the microelectrode and the gate sensitive radius on the terms were also simulated.

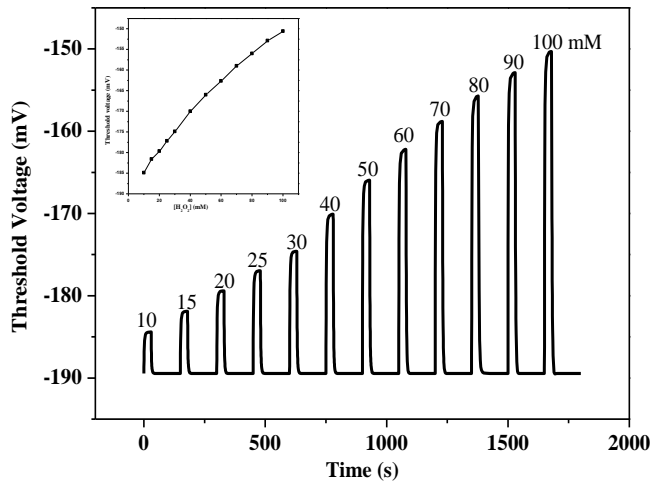


Fig. 8. Temporal variations of the pH-ChemFET threshold voltage for the different  $H_2O_2$  concentrations at  $0.7V$ ,  $t_p=30s$ ,  $d=50\mu m$ ,  $w=100\mu m$  and  $r_e=10\mu m$  and (inset)  $H_2O_2$  response of the ElecFET microdevice ( $V_p=0.7V$ )

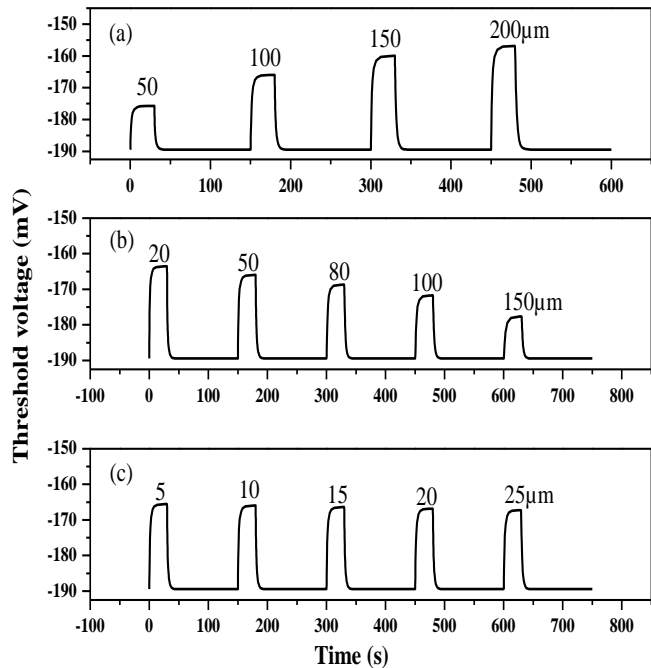


Fig. 9. Temporal variations of the pH-ChemFET threshold voltage for various: (a) surface of the microelectrode at  $d=50\mu m$  and  $r_e=10\mu m$  (b) positions of the microelectrode at  $w=100\mu m$  and  $r_e=10\mu m$ , and (c) gate sensitive radius at  $d=50\mu m$  and  $w=100\mu m$  and to all at  $V_p=0.7V$ ,  $t_p=30s$ ,  $[H_2O_2]=50mM$ .

The results of these simulations are shown in Fig. 8. It is worth noting that in Fig. 9, each of the three curves includes the results of simulations for  $V_p=0.7V$ ,  $t_p=30s$  and  $[H_2O_2]=50mM$ .

In Fig. 9a, the change of the threshold voltage is imposed by the variation of the microelectrode width ( $w$ ), from 50 to 200  $\mu m$  with a step of 50  $\mu m$ . In this case, the maximal variation  $V_T^{Sat}$  was increased during the simulation of this stage. Far from the microelectrode ( $d=20, 50, 80, 100$  and  $150\mu m$ ), once hydronium ions are created, they take longtime to diffuse into the solution causing a reduction in their number at very large distances leading to low response of the sensor as illustrated in Fig. 9b.

Finally, Fig. 9c shows the threshold voltage variation with time at various gate sensitive radius ( $r_e=5, 10, 15, 20$  and  $25\mu m$ ). When the gate sensitive radius increases, the  $V_T^{Sat}$  value also decreases slightly. This proves that the ElecFET detection principles depend mainly on the spatial integration of both microelectrode and pH-ChemFET microdevices.

### C. Comparison with experimental results

This section presents a comparative study of experimental results and those obtained by simulation (Fig.8) in the case of hydrogen peroxide detection. It is worth noting that our ChemFET-meter measurement interface was used to measure the pH-ChemFET gate-source voltage  $V_{GS}$ , also called output voltage  $V_{out}$ , enabling the local pH monitoring in the microelectrode surroundings depending on the polarization conditions.  $V_{out}$  shift provides an identical threshold voltage shift and therefore thinking in term of  $V_{out}$  or threshold voltage is the same.

Fig.10 shows the evolution of the output voltage versus time at various  $[H_2O_2]$  concentrations, while inset represents the maximum of  $V_{out}$  versus  $[H_2O_2]$  concentrations. We can see that the curve of sensor response for experimental studies shows similar shape as in theoretical studies. As the  $[H_2O_2]$  concentrations increases, the sensor response increases too, with  $V_{out}$  shifted towards positive values.

Our numerical results show that the amplitude of the impulsional voltage variations increases with the  $[H_2O_2]$  concentration in solution, and saturates for the highest values. This saturation phenomenon is related to the ElecFET detection principles as previously mentioned: in the presence of hydrogen peroxide, a positive bias on the platinum microelectrode produces hydronium  $H_3O^+$  ions. Therefore the local pH decreases and finally the pH-ChemFET-meter output voltage  $V_{out}$  increases. When the  $[H_2O_2]$  concentration increases, the  $H_3O^+$  ions production also increases. Nevertheless, the  $H_3O^+$  ion increase is limited by diffusion and electromigration phenomena, leading to a new chemical equilibrium at the microscale. Hydrogen peroxide  $H_2O_2$  potentiometric detection was finally demonstrated in the  $[10-100mM]$  range.

The response from our simulation is not in the same range of the value obtained from the experience. This is due to the effect of the buffer properties. Indeed, Chong et al. have shown that when concentration of the PBS solution decreases, the ionic strength of the PBS solution also decreases causing

the drain current  $I_d$  to decrease. The dependence of the  $I_d$  to the pH value of the testing pH buffer solutions is related to the variation of the threshold voltage [34]. In the future work, we intend to take into account the effect of the buffer.

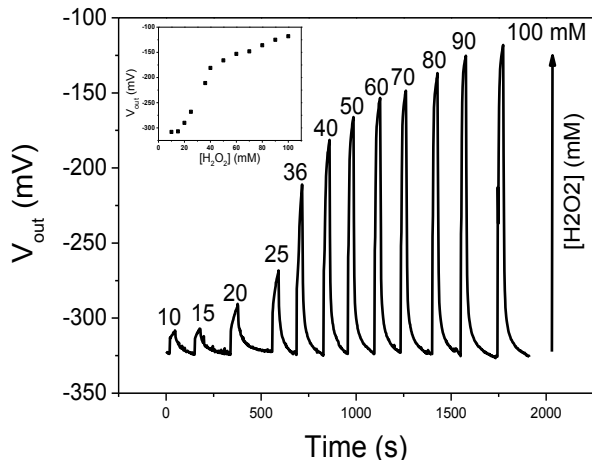


Fig. 10. Detection of impulsional pH variations related to the  $H_2O_2$  electrolysis in phosphate buffer solutions: influence of the  $H_2O_2$  concentration and (inset) ElecFET response for the  $H_2O_2$  detection.

#### IV. CONCLUSION

In this study, we have investigated the modelling of the ElecFET microdevice, taking into account the mass transport for different species, electrochemical reactions on the microelectrode and acid/basic reactions for couples ( $H_3O^+/H_2O$ ) and ( $H_2O/OH^-$ ). The pH-ElecFET techniques were used for monitoring the water-based electrolysis by pH-ChemFET and extended to the hydrogen peroxide in order to obtain the threshold voltage (i.e local pH) variation. The influence of the ElecFET geometrical design, i.e. characteristic width of the microelectrode  $w$ , gate sensitive radius  $r_e$  and distance between the gate sensitive radius and the microelectrode  $d$ , as well as polarization parameters, i.e. polarization voltage  $V_p$  and time  $t_p$ , on its response behavior was studied. So, the obtaining of pH impulsional variations in microvolumes was clarified and the potentiometric detection of hydrogen peroxide  $H_2O_2$  was evidenced in the [10–100mM] concentration range. In the near future, we intend to model the ElecFET device for the enzymatic detection of lactate and glucose in cylindrical coordinates.

#### REFERENCES

- [1] S. A. Zaidi, J. H. Shin, "Recent developments in nanostructure based electrochemical glucose sensors," *Talanta*, vol. 149, pp. 30–42, 2016.
- [2] S. Chaiyo, E. Mehmeti, K. Zagar, W. Siangproh, O. Chailapakul, K. Kalcher, "Electrochemical sensors for the simultaneous determination of zinc, cadmium and lead using a Nafion/ionic liquid/graphene composite modified screen-printed carbon electrode," *Analytica Chimica Acta*, 2016 (in press).
- [3] A. A. Vasiliev, A. V. Pisiakov, A. V. Sokolov, N. N. Samotaev, S. A. Soloviev, K. Oblov, V. Guarnieri, L. Lorenzelli, J. Brunelli, A. Maglione, A. S. Lipilin, A. Mozalev, A. V. Legin, "Non-silicon MEMS platforms for gas sensors," *Sensors and Actuators B* 224 (2016) 700–713.
- [4] A. Safavi, Z. Shojaeifard, M. Tohidi, "Fabrication of an Amperometric Sensor for Hydroxylamine Based on Silver Paste Nanocomposite Electrode," *IEEE Sensors Journal*, Vol. 14, pp. 839–846, 2014.
- [5] S. M. Sayyah, M. Shaban, M. Rabia, "A High-Sensitivity Potentiometric Mercuric Ion Sensor Based on m-Toluidine Films," *IEEE Sensors Journal*, vol. 16, pp. 1541–1548, 2016.
- [6] Y. Chen, S. C. Mun, J. Kim, "A Wide Range Conductometric pH Sensor Made With Titanium Dioxide / Multiwall Carbon Nanotube / Cellulose Hybrid Nanocomposite," *IEEE Sensors Journal*, vol. 13, pp. 4157–4162, 2013.
- [7] G. Alberti, F. Cherubini, R. Palombi, "Potentiometric and amperometric gas sensors based on the protonic conduction of layered zirconium phosphates and phosphonates," *Sensors and Actuators B*, vol. 24, pp. 270–272, 1995.
- [8] A.K. Diallo, L. Djeghlaf, J. Launay, P. Temple-Boyer, "Development of pH-based ElecFET biosensors for lactate ion detection," *Biosensors and Bioelectronics*, vol. 40, pp. 291–296, 2013.
- [9] A. K. Diallo, L. Djeghlaf, L. Mazonq, J. Launay, W. Sant, P. Temple-Boyer, "Modelling of impulsional pH variations using ChemFET-based microdevices: application to hydrogen peroxide detection," *Sensors*, vol. 14, pp. 3267–3283, 2014.
- [10] Y. Ouyang, X. Wang, G. Yu, Z. Song, X. Zhang, "Performance of Amperometric and Potentiometric Hydrogen Sensors," *J. Mater. Sci. Technol.*, vol. 30, pp. 1160–1165, 2014.
- [11] B.H. van der Schoot, P. Bergveld, *Biosensors*, vol. 2, pp. 161–186, 1988.
- [12] J. Luo, W. Olthuis, B. H. van der Schott, P. Bergveld, M. Bos, W. E. van der Linden, "Modelling of the migration effect occurring at an ISFET-based coulometric sensor-actuator system," *Anal. Chim. Acta*, vol. 237, pp. 71–81, 1990.
- [13] W. Olthuis, B.H. van der Schoot, F. Chavez, P. Bergveld, *Sensors Actuators*, vol. 17, pp. 279, 1989.
- [14] B.H. van der Schoot, P. Bergveld, *Sensors Actuators*, Vol. 13, pp. 251, 1988.
- [15] A. Meena, L. Rajendran, "Mathematical modeling of amperometric and potentiometric biosensors and system of non-linear equations-Homotopy perturbation approach," *Journal of Electroanalytical Chemistry*, vol. 644, pp. 50–59, 2010.
- [16] C. López-Gándaraa, M. Blanes, J.M. Fernández-Sanjuána, F.M. Ramosa, A. Cirera, "Modeling and optimization of diffusive layers in potentiometric and amperometric electrochemical gas sensors," *Procedia Engineering*, vol. 47, pp. 1295–1298, 2012.
- [17] W.E. Morf, P.D. van der Wal, E. Pretsch, N.F. de Rooij, "Theoretical treatment and numerical simulation of potentiometric and amperometric enzyme electrodes and of enzyme reactors Part 1: Steady-state concentration profiles, fluxes, and responses," *Journal of Electroanalytical Chemistry*, vol. 657, pp. 1–12, 2011.
- [18] W. E. Morf, P.D. van der Wal, E. Pretsch, N.F. de Rooij, "Theoretical treatment and numerical simulation of potentiometric and amperometric enzyme electrodes and of enzyme reactors. Part 2: Time-dependent concentration profiles, fluxes, and responses," *Journal of Electroanalytical Chemistry*, vol. 657, pp. 13–22, 2011.
- [19] G. Pardon, W. van der Wijngaart, "Modeling and simulation of electrostatically gated nanochannels," *Advances in Colloid and Interface Science*, vol. 199, pp. 78–94, 2013.
- [20] M. Moritsuka, Y. Kitasako, M.F. Burrow, M. Ikeda, J. Tagami, "The pH change after HCl titration into resting and stimulated saliva for a buffering capacity test," *Australian Dental Journal*, vol. 51, pp. 170–174, 2006.
- [21] K. Saeedfar, L. Y. Heng, T. L. Ling and M. Rezayi, "Potentiometric Urea Biosensor Based on an Immobilised Fullerene-Urease Bio-Conjugate," *Sensors*, vol. 13, pp. 16851–16866, 2013.
- [22] M. Alqasameh, L. Y. Heng, M. Ahmad, A. S. Santhana Raj and T. L. Ling, "A Large Response Range Reflectometric Urea Biosensor Made from Silica-Gel Nanoparticles," *Sensors*, vol. 14, pp. 13186–13209, 2014.
- [23] P. Temple-Boyer, J. launay, I. Humenyuk, T. Do Conto, A. Martinez, C. Bériet, A. Grisel, "Study of front side connected chemical field effect transistor for water analysis," *Microelectron. Reliability*, vol. 44, pp. 443–447, 2004.
- [24] Comsol multiphysics finite element analysis software, <http://www.comsol.com>.
- [25] L. Bousse, N. De Rooij, P. Bergveld, "Operation of chemically sensitive field effect sensors as a function of the insulator-electrolyte interface," *IEEE Trans. Electron Devices*, vol. 30, pp. 1263–1270, 1983.
- [26] A. Poghosian, "Determination of the  $pH_{pzc}$  of insulators surface from capacitance-voltage characteristics of MIS and EIS structures," *Sens. Actuators B*, vol. 44, pp. 551–553, 1997.
- [27] P. Temple-Boyer, J. Le Gal, M.L. Pourciel-Gouzy, W. Sant, A. Martinez, "Modelling of EnFETs for the creatinine detection," *Sensors and Actuators B*, vol. 118, pp. 47–52, 2006.
- [28] W. Sant, P. Temple-Boyer, E. Chanié, J. Launay, A. Martinez, "On-line monitoring of urea using enzymatic field effect transistors," *Sensors and Actuators B*, vol. 160, pp. 59–64, 2011.



- [29] Z. Dong, U.C. Wejiny, I.H. Elhajj, "Fabrication and testing of ISFET based pH sensors for microliter target solutions," *Sensors and Actuators A*, vol. 194, pp. 181–187, 2013.
- [30] M. Selmi, F. Echouchene, M. H. Gazzah, and H. Belmabrouk, "Flow Confinement Enhancement of Heterogeneous Immunoassays in Microfluidics," *IEEE SENSORS JOURNAL*, vol. 15, no. 12, 2015.
- [31] Nitesh Nama, Rune Barnkob, Zhangming Mao, Christian J. Kähler, Francesco Costanzo, and Tony Jun Huang, "Numerical study of acoustophoretic motion of particles in a PDMS microchannel driven by surface acoustic waves," *Lab on a Chip*, vol. 15, pp. 2700-2709, 2015
- [32] A.J. Bard, L.R. Faulkner, "Electrochemical methods: fundamental and applications", *second edition*, New York: John Wiley & Sons, Inc., 2001.
- [33] W. J. Moore, "Basic Physical Chemistry," *Prentice-Hall International Editions*, London, 1983.
- [34] Chong Soon Weng, U. Hashim, Wei-Wen Liu, "The Effect of Phosphate Buffer Solution (PBS) Concentration on the Ion Sensitive Field-Effect Transistor (ISFET) Detection", RSM2013 Proc., Langkawi, Malaysia, 2013.



**Nejiba Aoun** was born in Tunisia, 1984. She received his Master's Degree in Materials, Nano-structures, Device and Micro-electronics System from the Faculty of Science of Monastir, Tunisia in 2011. She is now a Ph.D. student at the laboratory of electronics and microelectronics, department of Physics, Faculty of science of Monastir. His research interests are modelling and simulation of microsensors.



**Fraj Echouchene** was born in Tunisia, 1978. He received Master and Ph.D. degree in Physical department from Monastir University in 2006 and 2011, respectively. In september 2012, he joined the Department of Physics at Gafsa University, Tunisia where he is assistant professor now. His research interests are modelling and simulation of microfluidic sensors, cavitation flow and heat transfer.



**Hafedh Belmabrouk** received the Ph.D. degree in laser Doppler velocimetry from the Ecole Centrale de Lyon, France, in 1992. He currently supervises a team of about 20 researchers in the field of nonlinear optics, biosensor and microfluidics, and heat transfer



**Abdou Karim Dialo** was born on April 14, 1977. He received his Master's Degree in Microelectronics from Louis Pasteur University of Strasbourg, France in 2005. He joined the Lyon Institute of Nanotechnologies, France in 2005 and received the Ph.D. degree from the Ecole Centrale de Lyon in 2008. He was a postdoctoral fellow at the French "Université de la Méditerranée" (France) in

the French "Centre Interdisciplinaire des Nanosciences de Marseille" (France) where he worked on organic transistor devices in 2009, and joined the French "Laboratoire d'Analyse et d'Architecture des Systèmes" of the French "Centre National de la Recherche Scientifique (LAAS-CNRS) as a postdoctoral fellow in 2010. He is working on the development of ChemFET-based microsensors for chemical and biochemical detections.



**Jérôme Launay** was born on March 1975. He received the Engineer Degree in electronic engineering from the French "Institut National des Sciences Appliquées de Toulouse" (INSAT-France) in 1998. He joined the French "Laboratoire d'Analyse et d'Architecture des Systèmes" from the French "Centre National de la Recherche Scientifique" (LAAS-CNRS) in 1998 and

received the Ph.D. degree from the French "Institut National des Sciences Appliquées de Toulouse" (INSAT-France) in 2001. In 2002, he became lecturer at the French "Université Paul Sabatier de Toulouse" (France). His research activities include the development of chemical microsensors for the detection in liquid phase.



**Pierre Temple-Boyer** was born on October 25, 1966. He received his Engineer Degree in electronic engineering from the Ecole Supérieure d'Electricité (Paris - France) in 1990 and his Master Degree in microelectronics from the French "Université Paul Sabatier de Toulouse" (France) in 1992. He joined the French "Laboratoire d'Analyse et d'Architecture des Systèmes" of the French "Centre National de la Recherche Scientifique" (LAAS-CNRS) in 1992 and received the Ph.D. degree from the French "Institut National des Sciences Appliquées de Toulouse" (France) in 1995. Since then, as a senior researcher, he has been working on the development of micro-and nanotechnologies.